Immunity, Volume *44*

Supplemental Information

In Vivo Killing Capacity of Cytotoxic T Cells Is Limited and Involves Dynamic Interactions and T Cell Cooperativity

Stephan Halle, Kirsten Anja Keyser, Felix Rolf Stahl, Andreas Busche, Anja Marquardt, Xiang Zheng, Melanie Galla, Vigo Heissmeyer, Katrin Heller, Jasmin Boelter, Karen Wagner, Yvonne Bischoff, Rieke Martens, Asolina Braun, Kathrin Werth, Alexey Uvarovskii, Harald Kempf, Michael Meyer-Hermann, Ramon Arens, Melanie Kremer, Gerd Sutter, Martin Messerle, and Reinhold Förster

Figure S1

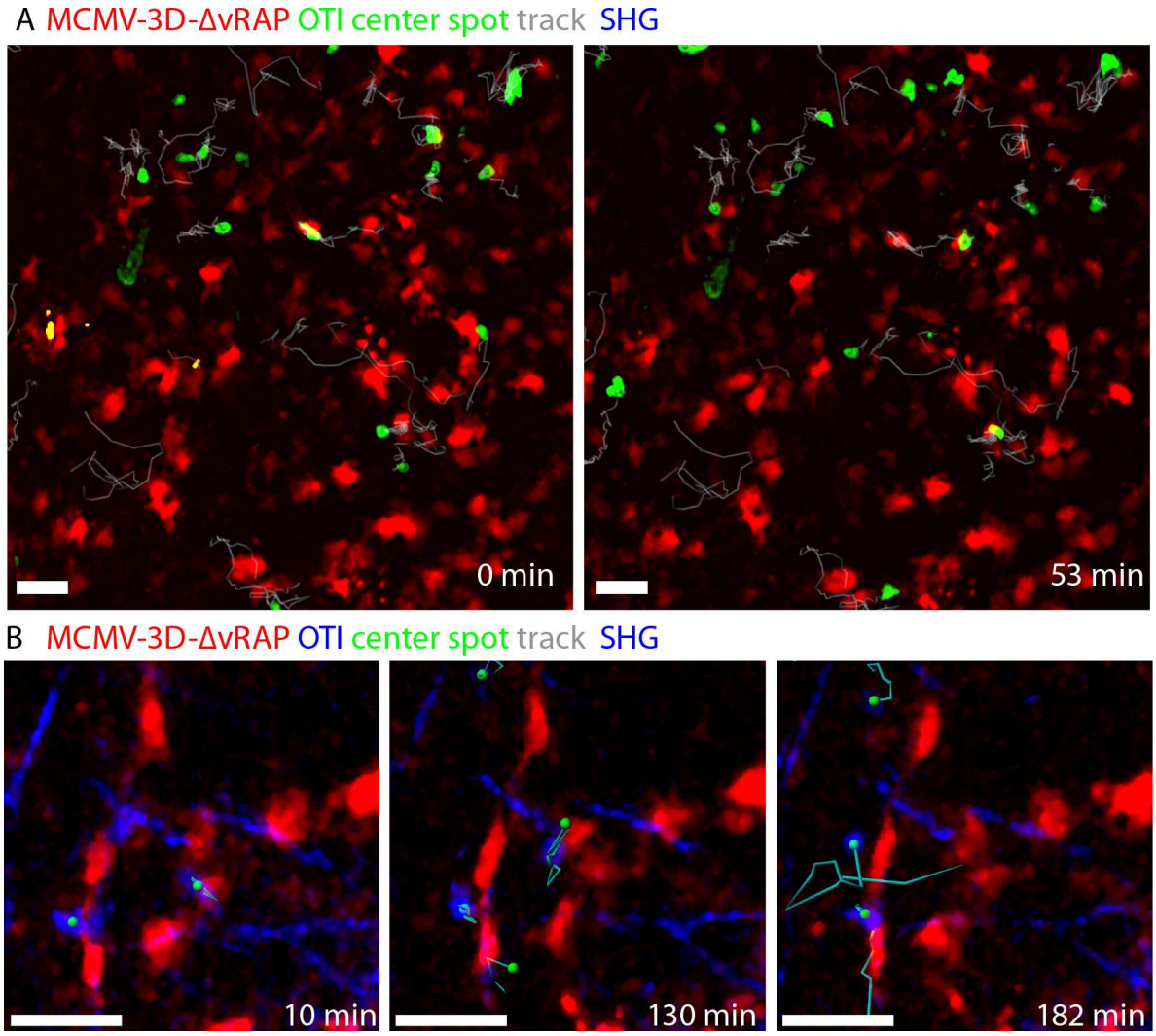

Figure S1, related to Figure 3. Virus-infected cells are not disrupted within minutes when only few virus-specific CTLs are present at the site of infection. (**A**) MCMV-3D-ΔvRAP-infected cells (red) were observed during imaging in regions with few OT-I CTLs (green) present (elapsed time in minutes). (**B**) In a movie with few CFP-OT-I CTLs (blue), virus-infected cells were followed over three hours (green center spots of tracked cells; gray tracks; SHG, blue; Movie S1). Scale bars, 30 µm. CTL were primed with SIINFEKL and poly(I:C). Pictures shown in A and B are derived from Movie S1.

Figure S2

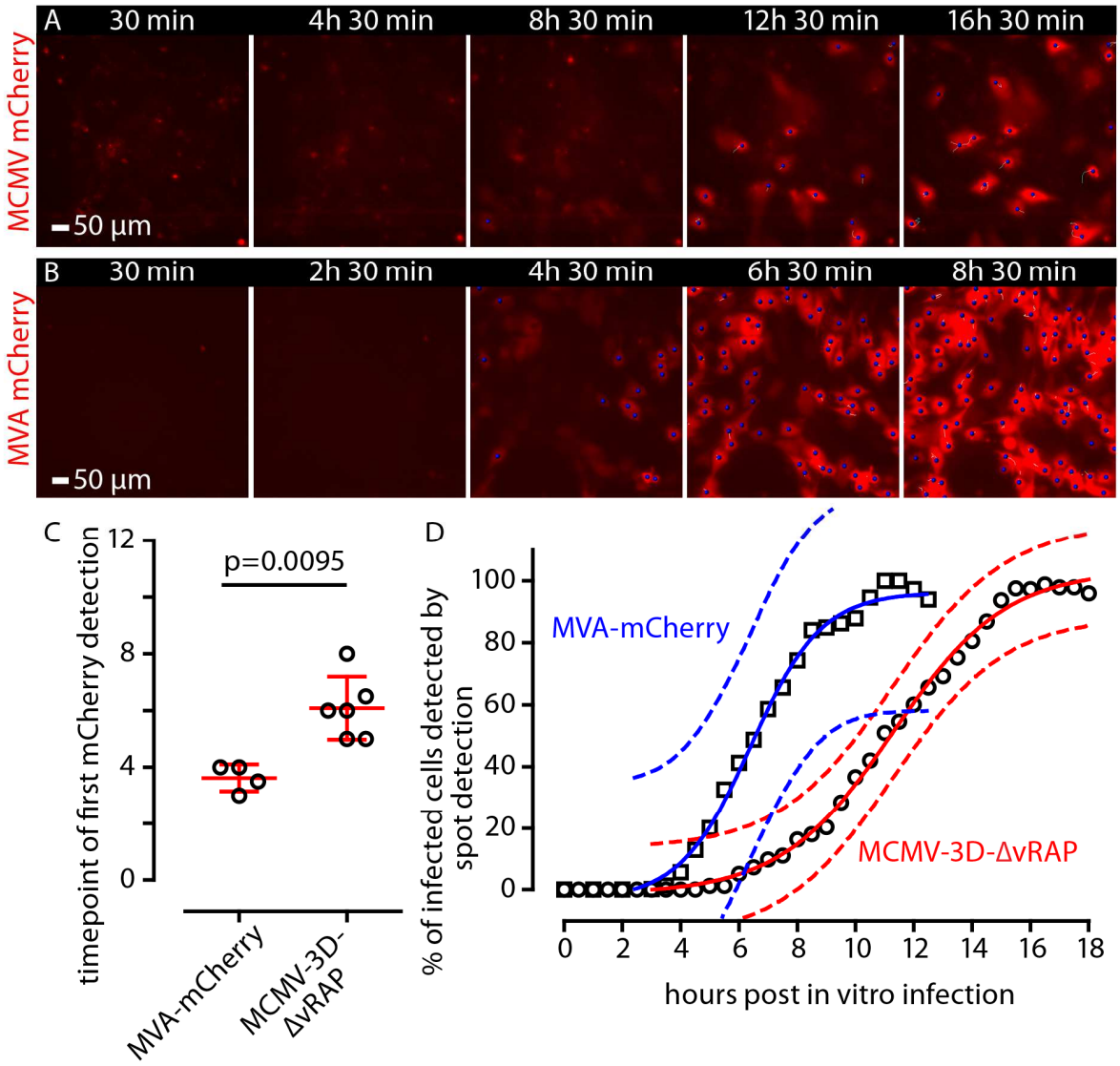

Figure S2, related to Figure 4. Time-lapse microscopy reveals early expression of virus-encoded mCherry. (**A**) C57BL/6 mouse stromal cells were infected *in vitro* with MCMV-3D-ΔvRAP at a MOI of 5-10 (A) or MVA-mCherry at a MOI of 5-10 (**B**). Single cell mCherry fluorescence intensities were monitored by time-lapse live cell microscopy between 30 minutes to 16 hours after infection. Scale bars, 50 µm. Blue spots, automatic detection of infected cells. (**C**) Time of first mCherry detection for the viruses indicated. Dots, movies; lines, mean and standard deviation; p-value, Mann-Whitney test. (**D**) Automated spot detection was used to track mCherry-expressing cells over time. The percentage of the number of detectable cells was plotted over time. Data pooled from 4 experiments; line, sigmoidal dose response curve fitted; dotted lines, 95% prediction interval for the viruses indicated. Pictures shown in A and B are derived from Movie S4.

Figure S3

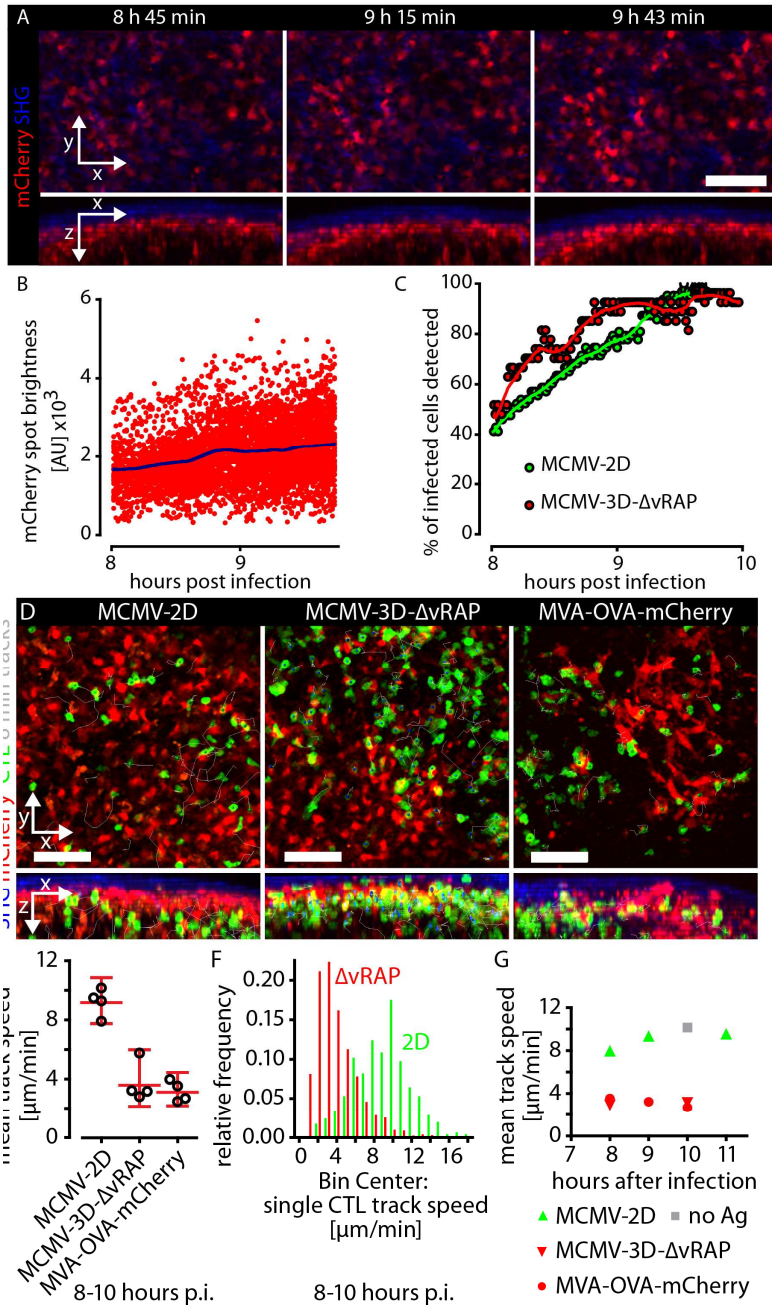

Figure S3, related to Figure 4. SIINFEKL and mCherry are both expressed early after virus infection. (**A**) Mouse popliteal lymph nodes were explanted 8 hours after virus injection into the footpad. Lymph node collagen fibers (blue, SHG) and virus-expressed mCherry (red) were detected by 2-photon microscopy at regular laser intensity. Scale bar, 50 µm. x-z views are shown to control for tissue drift during imaging. (**B**) All mCherry$^+$ cell spots were automatically detected and the mCherry brightness was plotted over time. Blue line, locally weighted scatter-plot smoothing curve. (**C**) For both MCMV-2D and MCMV-3D-ΔvRAP-infected lymph nodes, mCherry-intensity was plotted for the time points indicated after infection. Data shown are representative of 4 independent experiments. Line, locally weighted scatter-plot smoothing curve. (**D**) At 8-10 hours after infection with the viruses indicated, GFP-expressing OT-I CTLs were observed at the site of infection in case the viruses encode the SIINFEKL epitope (middle and right panel). Compared to the images depicted in Figure S2, stronger contrast setting were used here for the mCherry channel. Pictures are representative of 5 independent 2-photon imaging experiments. Scale bars, 50 µm. (**E**) CTL track speed at the site of infection plotted for the three viruses shown in panel (D). (**F**) At 8-10 hours after infection with the indicated viruses, single CTL track speed data frequency distribution is shown from all analyzed CTLs. (**G**) CTL population track speed was analyzed at the time points indicated. Dots, mean values per time-point. Data pooled from 5 independent experiments. CTLs were primed with MVA-OVA.

Figure S4

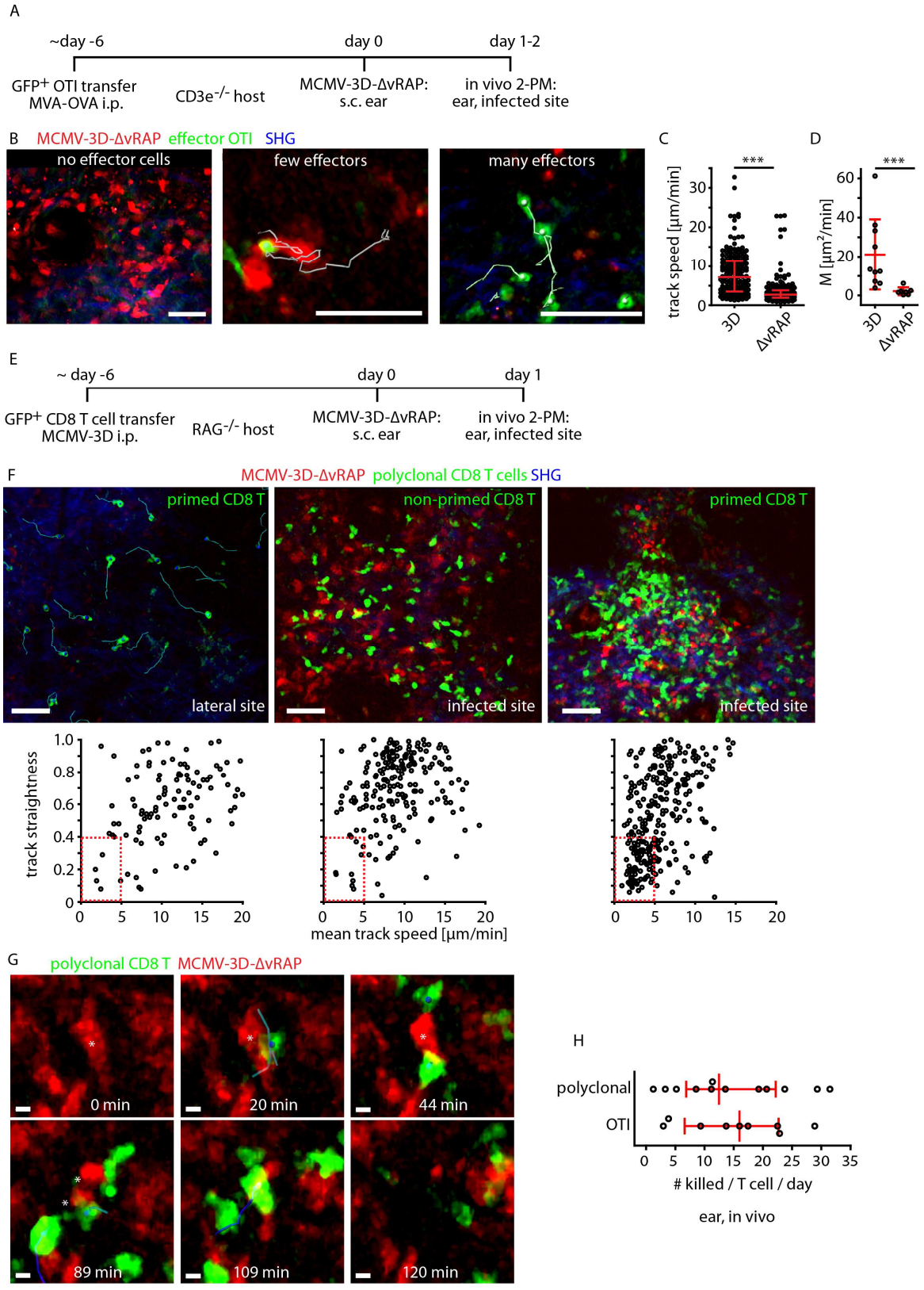

Figure S4, related to Figure 4. *In vivo* imaging of CTLs and MCMV-infected cells in the skin reveals low killing rates. (**A**) Protocol for intravital imaging of OT-I CTL in *Cd3ε*-deficient mice: GFP-expressing naïve OT-I were transferred and MVA-OVA was used to prime the SIINFEKL-specific antiviral response. (**B**) Following MCMV-3D-ΔvRAP infection in the ear, intravital imaging was used to visualize the infected cells in mice without CTLs (left), with few CTLs (middle) or many CTLs (right). OT-I CTL track speed (**C**) and motility coefficient (**D**) was analyzed during interaction of CTLs and infected cells. Dots, cells (C) and movies (D). Data pooled from 3 experiments; Mann-Whitney test. Scale bars, 20 µm. (**E**) Protocol for intravital imaging of *Rag2*$^{-/-}$

mice reconstituted with polyclonal FP-CD8$^+$ T cells and primed (MCMV-3D i.p.) or not primed six to seven days earlier. (**F**) Migratory behavior of FP-CTLs cells one day after secondary ear infection with MCMV-3D-ΔvRAP at conditions indicated. The percentage of cells in the boxed region was used as the percentage of MCMV-specific CTLs (lower panel: dots, cells; data from 1-4 movies collected in 6 independent experiments). (**G**) Polyclonal FP-CTLs contacted infected cells. Asterisks point to target disruption. (**H**) *In vivo* per capita killing rate of polyclonal or OT-I CTLs in the ear skin determined by intravital microscopy (dots, movies; pooled from 2 to 4 independent experiments). Scale bars, 50 µm (F) or 5 µm (G). Data shown in F and G are taken from Movie S5.

Figure S5

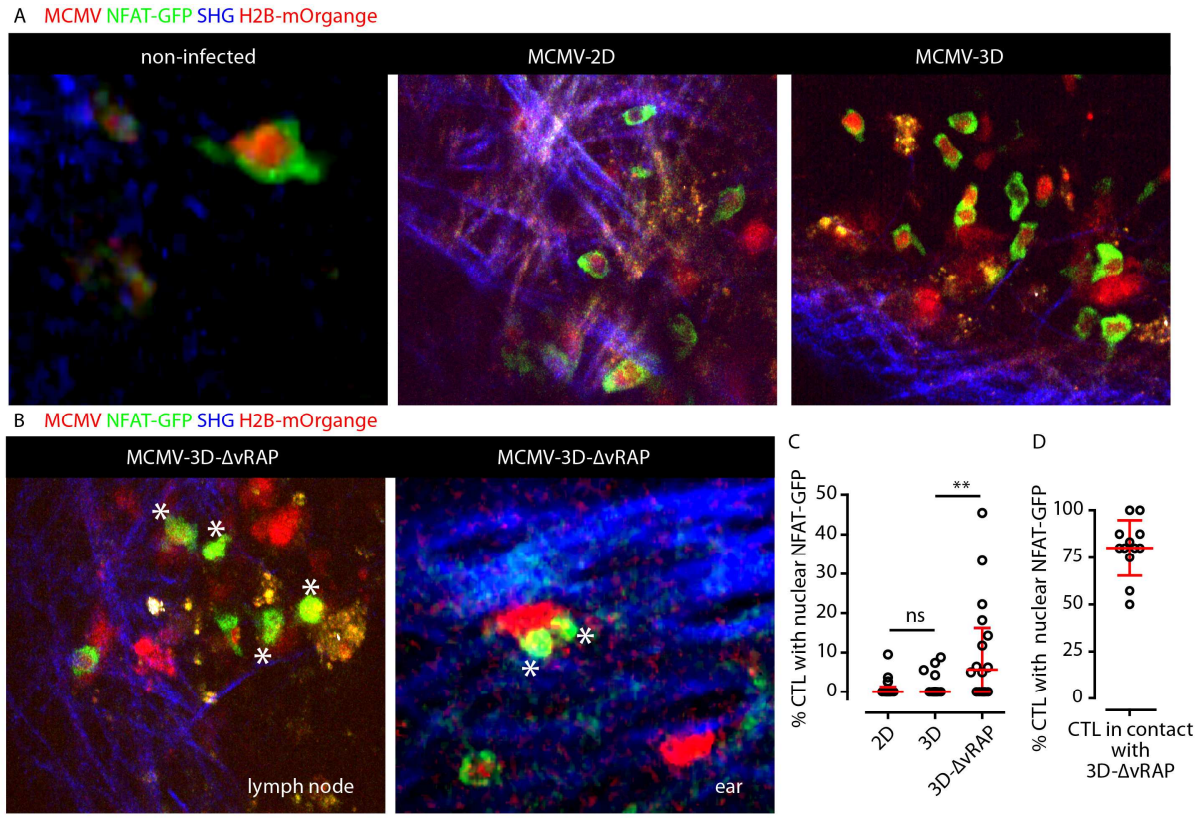

Figure S5, related to Figure 7. Viral immune evasion prevents NFAT signaling in virus-specific CTLs. NFAT-GFP and H2B-mOrange-expressing naïve OT-I CD8$^+$ T cells were transferred into mice followed by T cell priming and expansion by treatment with MVA-OVA. One week later, NFAT-GFP (green) and H2B-mOrange (red) CTLs were observed by 2-photon microscopy in non-infected lymph nodes, MCMV-2D or MCMV-3D-infected lymph nodes. (**A**) NFAT-OT-I CTLs showed a cytoplasmatic GFP signal that spared the mOrange$^+$ nucleus in lymph nodes infected with MCMV-2D or MCMV-3D. (**B**) In lymph nodes or ear dermis infected with MCMV-3D-ΔvRAP, NFAT-OT-I CTLs in contact with target cells showed a nuclear NFAT-GFP signal. (**C**) The percentage of NFAT-OT-I CTLs with a nuclear NFAT-GFP signal was analyzed for lymph nodes infected with MCMV-2D, MCMV-3D or MCMV-3D-ΔvRAP (dots, movies; data pooled from 19 lymph nodes from 3 independent experiments). (**D**) For the CTLs in contact with MCMV-3D-ΔvRAP-infected cells, the percentage of nuclear NFAT-GFP was analyzed (percentage of all CTLs in contact with MCMV-3D-ΔvRAP-infected cells; dots, movies; data pooled from 5 independent experiments). See also Movie S6.

Figure S6

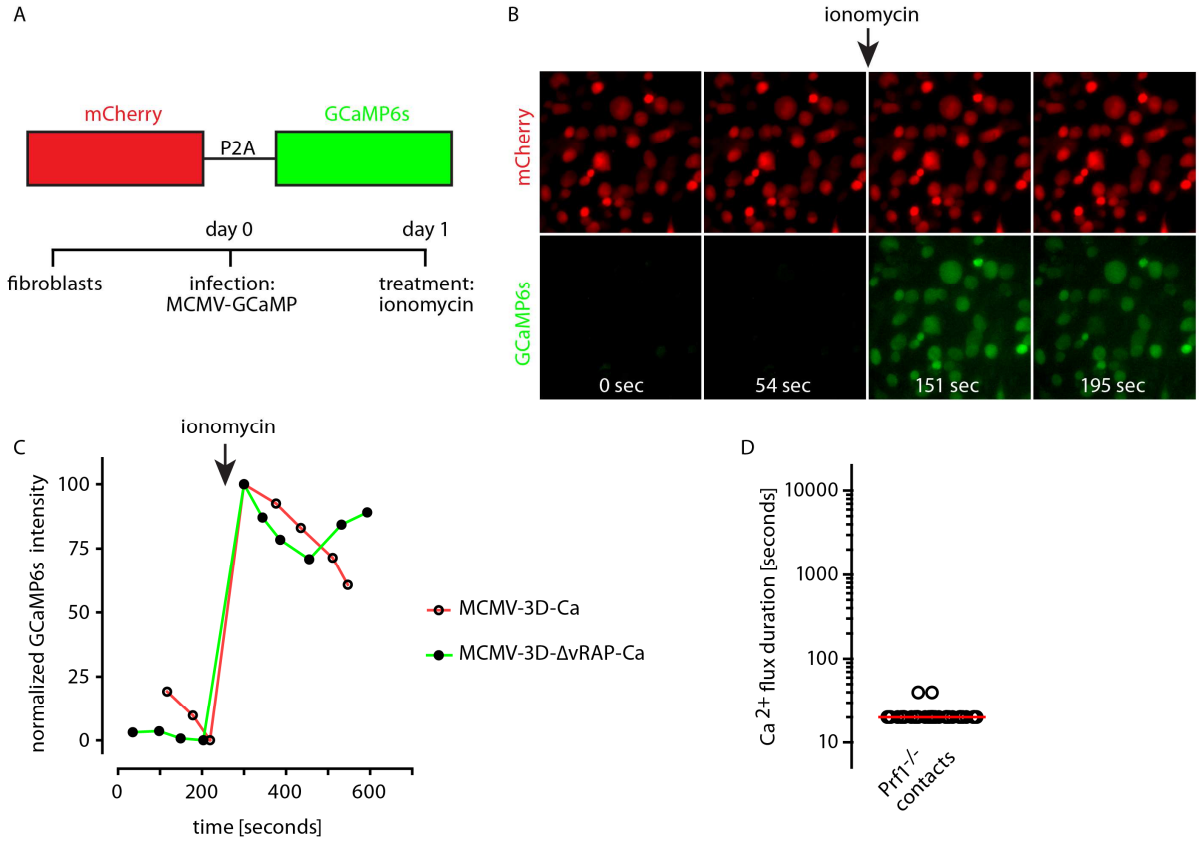

Figure S6, related to Figure 7. Viral expression of GCaMP6s allows for visualization of Ca^{2+}-signaling in virus-infected cells. (**A**) Mouse fibroblasts were infected *in vitro with* the MCMV-strains expressing mCherry and the GCaMP6s Ca^{2+}-sensor and treated with ionomycin. (**B**) *In vitro*, very low GCaMP6s-fluorescence (green) was observed before ionomycin treatment. Some infected cells showed spontaneous Ca^{2+} signals. Following ionomycin addition, all mCherry-expressing cells (red) showed a prolonged green fluorescent signal (observed in 4 experiments). (**C**) Normalized GCaMP6s-fluorescene intensity before and after ionomycin treatment *in vitro* (data pooled from 2 independent experiments). (**D**) Perforin-deficient CTLs were intra-lymphatically transferred and contact events with MCMV-3D-ΔvRAP-Ca-infected cells were analyzed (dots, flux events; 68 events analyzed in total, data pooled from 3 experiments with explanted lymph nodes). See also Movie S7.

Figure S7

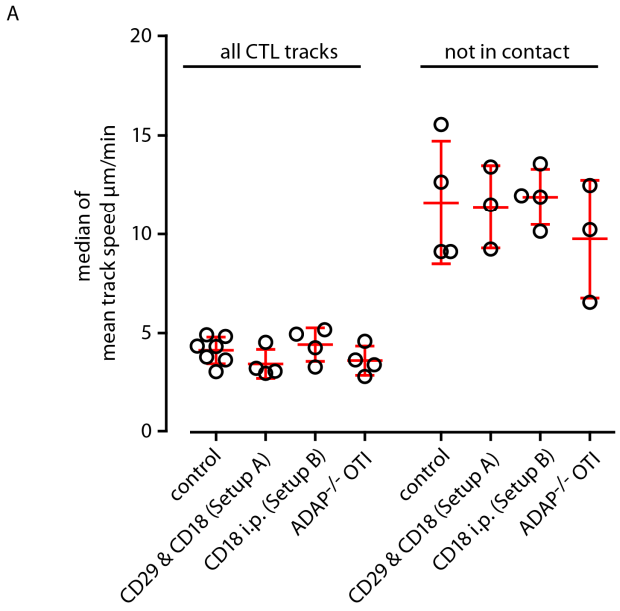

Figure S7, related to Figure 7. Virus-specific CTLs migrate slowly during attack on virus-infected cells independently of ADAP or integrin function. (**A**) Virus-specific OT-I CTLs "scanning" migration was analyzed after blockade of beta-1 and beta-2 integrins. CTL track speed was analyzed during attack on MCMV-3D-ΔvRAP-infected cells in the virus-infected region of the popliteal lymph node on one day after virus infection (all CTL tracks). Intra-lympatic transfer of non-treated (control group) or anti-CD29 and anti-CD18 treated CTLs (setup A) was performed. In setup B, the recipient mouse was treated with an intra-peritoneal injection of 400 µg of anti-CD18 antibody prior to CTL transfer. Data pooled form 4 independent experiments. *Adap*$^{-/-}$ OT-I CTLs were injected in two independent experiments. Explanted lymph nodes were imaged. CTLs were primed by MVA-OVA. All CTLs were tracked to allow direct comparison between groups (left; marked as "all CTL tracks"). To test whether CTLs that freely migrate and that are not in contact with virus-infected cells show the normal track speed of around 10 µm/min, these cells were identified and re-analyzed separately (right; marked as "not in contact"). Dots, median values of all CTLs per movie; Lines, mean; error bars, standard deviation; Kruskal-Wallis test p-value = 0.24 (all CTL tracks) and 0.82 (not in contact).

Supplemental Experimental Procedures

Murine cytomegalovirus (MCMV) strains: All MCMV strains were derived from BAC pSM3fr cloned Smith strain, as described previously (Marquardt et al., 2011). Notably, all MCMV strains used in this study do not express m157, which is a natural killer cell-activating viral protein in B6 mice. MCMV stocks were generated by ultracentrifugation through a sucrose cushion and titrated on murine fibroblasts, yielding comparable plaque-forming units (PFU) per ml stock across all virus preparations used. The MCMV-3D-Ca and MCMV-3D-ΔvRAP-Ca BACs were derived from the MCMV-3D and MCMV-3D-ΔvRAP BACs (Marquardt et al., 2011), employing the *en passant* mutagenesis protocol (Tischer et al., 2010). Briefly, a kanamycin resistance (KanR) cassette (including an I-SceI site and a sequence duplication required for subsequent deletion of KanR) was inserted at the 3'-end of the ORF of the Ca^{2+}-binding protein calmodulin (CaM) in plasmid pGP-CMV-GCaMP6s (Chen et al., 2013) obtained from Addgene (plasmid #40753). The CaMP6s-KanR cassette was amplified using primers with homologies to the P2A and SV40p(A) signal sequences present within the MCMV-3D and MCMV-3D-ΔvRAP BACs. PCR products were transfected into *E. coli* GS1783 cells containing either one of the respective BACs and the KanR cassette was excised after successful insertion.

Modified Vaccinia virus Ankara (MVA) strains: Recombinant MVA-OVA viruses have been described previously (Halle et al., 2009; Lehmann et al., 2009). MVA-mCherry and MVA-OVA-mCherry were generated by homologous recombination using the plasmid vectors pIIIdHR-P7.5 and pLW-73 according to standard procedures (Kremer et al., 2012). The mCherry coding sequence was inserted in the I8R/G1L intergenic site, under transcriptional control of the vaccinia virus-specific synthetic early-late promoter PmH5. The ovalbumin gene was placed at the site of deletion III in the MVA genome and expressed by the natural viral early-late promoter P7.5. All MVA viruses were amplified and titrated on primary chicken embryonic fibroblasts. High titer MVA stocks were obtained by ultracentrifugation through sucrose and stored in 1 mM Tris-HCl pH 9.0 at -80°C.

Mouse infection models: Mice were anaesthetized by intraperitoneal (i.p.) injection of ketamine (100 mg/kg) and xylazine (5 mg/kg) and subsequently injected subcutaneously (s.c.) into the hind footpad (or the ear) with 10^6 PFU of the different MCMV strains diluted in 25-50 µl phosphate buffered saline (PBS). For MVA infections, 10^7 PFU of virus were diluted in 25-50 µl PBS and injected s.c. into the hind footpad. The time of virus injection was defined as time of infection.

Generation of OT-I CTLs *in vivo*: Lymphocytes from CD45.1$^+$ FP-OT-I mice, containing 10^5 CD8$^+$ TCR Vα5$^+$ OT-I cells, were injected i.p. or i.v. into recipient male C57BL/6, into *Cd3ε*-deficient or perforin-deficient mice. One day later, FP-OT-I cells were activated *in vivo* by vaccination with 17 µg SIINFEKL-peptide injected i.p., together with 85 µg poly(I:C) (Sigma). Alternatively, s.c. footpad injection of 50 µg OVA-protein (Sigma) together with MVA-wt as an adjuvant, or SIINFEKL peptide plus incomplete Freund's adjuvant (IFA, Sigma), was used to generate effector FP-OT-I cells. In some experiments, *Cd3ε*$^{-/-}$ mice that lack any endogenous T cells were used as recipients in combination with 10^4-10^5 FP-OT-I transferred before MVA-OVA i.p. priming with 1-5x10^6 PFU per mouse.

Generation of MCMV-specific CTLs from the endogenous repertoire: To generate MCMV-specific CTLs, naïve GFP- or CFP-expressing B6 mice were i.p. infected with 10^6 PFU MCMV-3D, and lymphoid organs were harvested 6 - 8 days later. Next, CD8$^+$ T cells were enriched by negative selection (MACS). Subsequently, 2 – 5 x10^6 CD8$^+$ T cells were stained with M45$_{985\text{-}993}$ D^b tetramer (Munks et al., 2006) and positively selected using anti-biotin magnetic beads. Approximately 60% of selected cells were CD8$^+$CD44$^+$ M45-labelled CTLs. MHC-I tetramers were prepared as described (Altman et al., 1996). Alternatively, bulk effector CD8$^+$ T cells (poly-specific for different MCMV-epitopes) were labeled with TAMRA or CMFDA (CellTracker green, Thermo Fisher Scientific) and enriched for effector cells by depleting CD62L^{hi} naïve CD8$^+$ T cells by MACS, yielding 60-70% CD8$^+$ CD44^{hi} T cells. For FACS sorting, M45-, M38- and m139-tetramer-binding CD8$^+$ T cells were selected from MACS-purified CD8$^+$ T cells, yielding 90% CD8$^+$CD44$^+$tetramer$^+$ CTLs used for CMFDA-labelling and intra-lymphatic delivery. For intravital imaging, CD8$^+$ MACS-purified GFP-B6 cells were transferred into *Rag2*-deficient mice, followed by i.p. primary infection with 10^6 PFU MCMV-3D.

Cell culture: Human 293T and murine SC-1 cells were grown in High-glucose [4.5 g/L] Dulbecco's modified Eagles medium including stable glutamine (DMEM; Biochrom, Berlin, Germany) supplemented with 10% (v/v) fetal calf serum (FCS), 1 mM sodium pyruvate and 1% (v/v) Penicillin/Streptomycin (all PAA, Coelbe, Germany).

Cloning of the NFAT-GFP construct: Plasmids pRSF91.NFATeGFP.PRE*, encoding a fusion protein of amino acids 1-460 of mouse NFAT1 and eGFP, as well as pRSF91.synH2BmOrange.PRE* are derived from the gammaretroviral vector plasmid pRSF91.eGFP.PRE*. NFATeGFP (Aramburu et al., 1998) was introduced into

pRSF91.eGFP.PRE* by ligating the 957 bp (NcoI / BamHI) and 1152 bp (BamHI / BsrgI) fragments of pMSCV.NFATeGFP.Puro with the 4918 bp back bone fragment (NcoI / BsrgI) of pRSF91.eGFP.PRE*. To facilitate cloning of pRSF91.synH2BmOrange.PRE* we used gene synthesis (Integrated DNA Technologies, Leuven, Belgium) to introduce restriction sites Acc65I and AgeI upstream of the ATG start codon and to eliminate restriction sites BsrgI, BspmI and AgeI within the first 430 bp of H2B without changing the amino acid code. The synthesized product synH2B was introduced into pCDNA3.H2BmOrange (Addgene plasmid 20969, (Nam and Benezra, 2009) by ligating the 5388 bp (XbaI / Acc65I) and 681 bp (MscI / XbaI) fragments of pCDNA3.H2BmOrange with synH2B (Acc65I / MscI) resulting in plasmid pCDNA3.synH2BmOrange. Finally, the EGFP expression cassette of pRSF91.EGFP.PRE* was replaced by synH2BmOrange using restriction enzymes AgeI and BsrgI.

Gammaretroviral particles and generation of NFAT-GFP OT-I T cells: Gammaretroviral particles were produced as previously described (Galla et al., 2013). In brief, $5x10^6$ 293T cells were seeded in surface-treated 10 cm-culture dishes. The next day, cells were transfected with 5 µg pRSF91.NFATeGFP.PRE* or pRSF91.H2BmOrange.PRE* together with 7 µg pCDNA3.MLV.Gag/Pol and 3 µg pEnv(eco)-IRES-puro expression plasmids (kindly provided by T. Kitamura, Japan (Morita et al., 2000)) using the Ca^{2+} phosphate transfection method assisted by 25 µM chloroquine (Sigma Aldrich). Gammaretroviral supernatants were harvested 36 and 60 h post-transfection, filtered through a 0.22 µm filter (Millipore), pooled and overnight 50x concentrated via ultracentrifugation at 13,238 x g and 4°C. Gammaretroviral vector supernatants were titrated by transducing 1 x 10^5 SC-1 cells with serial dilutions of the concentrated supernatant in the presence of 4 µg / mL protamine sulfate (Sigma Aldrich) and centrifugation for 60 min at 400 x g and 30-37°C. Two days later, cells were analyzed by flow cytometry and the transducing units / mL of each supernatant was determined by using experiments showing transduction efficiencies below 30%. Bone marrow chimeric mice were generated by infecting OT-I mouse bone marrow cells with the gammaretroviral vector supernatants and transfer of NFAT-GFP-expressing cells into irradiated C57BL/6 recipients. 6 weeks later, NFAT-GFP expression in OT-I $CD8^+$ T cells was observed in blood cells by flow cytometry and mice showing the brightest NFAT-GFP signal were used as donors of naïve NFAT-GFP OT-I $CD8^+$ T cells.

Intra-lymphatic injection of CTLs: We intra-lymphatically (i.l.) transferred different numbers of CTLs 2 - 6 hours following MCMV-3D-ΔvRAP infection. Injection was performed as described before (Braun et al., 2011). Briefly, 2.5 x 10^4 – 1 x 10^5 CTLs diluted in 5 µl PBS were injected in 90 seconds into the afferent lymph vessel draining towards the popliteal lymph node.

Organ preparation: For histology, tissue was fixed in 2% PFA overnight and embedded in OCT compound (Tissue-Tek). For flow cytometry, single-cell suspensions were prepared by mechanical disruption. Cells were blocked with 5% rat serum, stained and analyzed with a LSRII cytometer (BD Biosciences). Data was analyzed using WinList 6.0 (Verity Software House). The following antibodies were used: CD8-beta-Cy5 (RMCD8-2), CD44-eFluor 450 (IM7), CD62L-biotin (MEL-14), CD169-Alexa647 (MOMA-1), CD11b-PE-Cy7 (M1/70), CD11b-PE (M1/70), CD69-PerCP-Cy5.5 (H1.2F3), CD45-APC or FITC (30-F11), CD18 (2E6), CD18 (M18/2), CD29 (Hmβ1-1).

Fluorescence microscopy: Unfixed organs were inspected directly after dissection under fluorescence illumination (Leica Macroscope). PFA-fixed organs were embedded in OCT compound, sections were rehydrated in Tris-buffered saline with 0.05% Tween-20 (Sigma), blocked with 2.5% rat and 2.5% mouse serum and stained at room temperature for 30 minutes. Pictures were taken using a Zeiss Axiovert fluorescence microscope and AxioVision 4.6 software (Carl Zeiss, Germany). All pictures were contrast adjusted. For time-lapse *in vitro* imaging, the microscope imaging chamber was heated to 37°C and cells were cultured in sealed Lab-Tek II chamber slides (Nalge Nunc International, USA) in RPMI medium with 10% FCS, 1% Penicilin-Streptomycin, 1% L-Glutamin and 10 mM Hepes.

2-photon microscopy: Explanted lymph nodes were immobilized in an imaging chamber using tissue adhesive (Surgibond) and superfused with oxygenated (95% O_2 with 5% CO_2) RPMI medium (Invitrogen, Thermo Fisher Scientific) containing 5 g/L D(+) glucose monohydrate (Sigma) as described (Halle et al., 2009). Lymph nodes (LN) were kept shortly at 4°C before imaging at 37.5°C. Explanted lymph nodes were stored for 5-20 min on ice in RPMI 1640. After a 15 min equilibration at 37.5°C, CTLs showed regular migration (not shown). For intravital imaging of the ear, anaesthetized mice were placed on a 37°C warm stage and the imaging region was covered with PBS. The following microscope setup was used for 2-photon imaging: TriM Scope (LaVision BioTec), Olympus BX51 upright microscope, 20× 0.95 NA water immersion objective, two Mai Tai Titanium:sapphire pulsed infrared lasers (Newport Corporation, Spectra-Physics). One Laser was tuned to 920 nm for excitation of GFP, CMFDA, CFP and TAMRA. The second Mai Tai laser was used to drive an optical parametric oscillator (OPO; APE, Berlin) to generate 1100 nm light to excite mCherry. To generate time-lapse series, Z-stacks of up to 10-18 images were acquired every 6 - 60 sec. 400 µm x 400 µm x 80 µm view fields of

the afferent side of the popliteal LNs were acquired. The same imaging region was used throughout this study, defined by the first B cell follicle visible on the cortical LN side, as determined by typical auto-fluorescence and shape. Data analysis of 2-photon imaging was performed using Imaris 7.2-8.0.1 (Bitplane). The presence of intact virus-infected cells was determined by manual inspection of every single infected cell in the single-slice visualization mode of the Imaris software. All movies were median-filtered for noise reduction. When needed, Imaris drift correction was applied. In all movies, the position of all virus-infected cells was checked in 3D over time to exclude loss of target cells by tissue drift. Tracking was done with cell diameters of 5 - 7 µm for T cells and 9-11 µm for virus-infected cells, maximum distance of 6 - 15 µm, gap size of 0 - 5 and manual inspection of tracks. When displayed, tracks are shown as cylinders or lines and center spots indicate the tracked cell at the current position. Real elapsed time is displayed in all movies. To quantify the number of virus-infected cells by 2-photon microscopy, we imaged a 400 µm x 400 µm x 80 µm volume, centered on the virus-infected site below the afferent subcapsular sinus. This imaging volume contained 50 ± 31 and 50 ± 23 (mean ± SD) virus-infected cells one day p.i. with MCMV-3D or MCMV-3D-ΔvRAP, respectively. For analysis of Ca^{2+} flux events, movies were drift corrected and the CTL contact start and end-points were recorded. In parallel, the start and end frames of bright GCaMP6s signals were recorded. A flux event observed to last over 30 seconds was called a "long-lasting" flux event. All long-lasting flux events were analyzed whether they followed a CTL contact and how much time had elapsed between CTL contact initiation and first frame of the bright GCaMP6s-signal. When virus-infected cells were disrupted, the mCherry-labelled remnants often showed a very long-lasting GCaMP6s-signal until the remnants disappeared.

Estimation of single CTL killing capacity from 2-photon movie datasets: To calculate the per capita killing rate (PCKR) of CTLs, we used Imaris spot detection to determine the number of effector cells per imaging volume during the first 10 time-points (the CTL number present at the start remained stable over time). Next, the number of infected cells was recorded at each time-point, yielding the number of infected cells killed. The average number of infected cells killed per CTL in 24 hours, i.e. the per capita killing rate (PKCR), was calculated as follows: $[(T_{start} - T_{end}) / E] \times 24 / t_{movie}$ (T_{start}, number of infected cells at beginning; T_{end}, number of infected cells at end of movie; E, number of effectors cells (mean CTL number from the first 10 time-points); t_{movie}, duration of the movie in hours). Note that the PCKR is normalized to the duration of 24 hours. The mathematical model is based on single-time-point pictures (taken 24 hours after infection and CTL i.l. transfer) and is described in detail below (Mathematical Model).

Analysis of CTL cooperativity: The pooled imaging data was compared against a null hypothesis that does not assume CTL cooperativity, that means, that simply states that the target cell death probability at each CTL contact is an independent event with a level of p(target cell death with single CTL contact)=0.14 (observed probability of target cell death upon single CTL attack). The probability of target cell death was plotted for infected cells that were contacted by zero to fourteen CTL. The p-values were calculated using the one-tailed exact binomial test.

Statistical analysis: Statistical analysis was performed with GraphPad Prism 4. When comparing two groups, p-values were calculated with the nonparametric Mann-Whitney test. To compare multiple groups, the Kruskal-Wallis test was used, in combination with Dunn's test. Error bars represent mean and standard deviation (SD), or median and inter-quartile range (IQR), as indicated. Linear regression analysis was used when a roughly linear relation was observed between two parameters. Non-linear regression analysis was performed fitting a one-phase exponential decay curve to the data. Three outliers are not displayed in Fig.5E, but included in the dataset for the Kruskal-Wallis test. To plot the one-phase exponential decay curve, two outliers (indicated by x) were excluded from regression analysis in Fig.6A. Where applicable, p-values are indicated in the figures as follows: *, $p<0.05$; **, $p<0.01$; ***, $p<0.001$. All experiments shown were performed at least twice. All mice were randomly assigned to treatment groups. Blinded outcome analysis was performed for data shown in Fig.6B and Figure S5C to exclude observer bias in quantification of infected cell numbers or NFAT-GFP scoring, respectively. All experimental data for each figure item are shown, there are no datasets for figure items that were analyzed but not presented.

Mathematical Model: The experimental data consist of the numbers of infected cells that survived after 24 hours in the presence of different T cell numbers following intra-lymphatic CTL transfer. The killing kinetics of T cells was described with a simple rate equation

$$\frac{dI}{dt} = -kTI$$

where I is the number of infected cells, T the number of T cells, and k is the parameter to be estimated. Such a model is based on the assumption that the probability of an infected cell to be killed by a T cell depends only on

the number of T cells, but not on the time. In the process of killing only one T cell participates, so no cooperative behavior was considered in this model. The number of infected cells at the time point *t* is

$$I(t) = I_0\, exp(-kTt)$$

where I_0 is the initial number of infected cells. We assume that cells can die only due to interaction with cognate effector CD8 T cells, since we did not observe any lysis of infected cells in the absence of T cells. The number of T cells is assumed to be constant during the whole experiment. Since there were two different scales of microscopy measurement, 400 µm x 400 µm and 500 µm x 500 µm, we scaled all the numbers to the 400 µm x 400 µm setup. We assume that the initial number of infected cells is log-normally distributed, $\log I_{exp} = \log I_0 - kTt + \epsilon$, where $\epsilon \sim N(0, \sigma)$. Four different killing rates *k* for every experimental condition and I_0 were estimated by multiple linear regression using R (R Core Team, 2015).

We consider zero values as censored measurements and use the substitute method to treat them (G.J. Nehls, 1973). Outliers were detected using robust regression as described in (Motulsky and Brown, 2006). For perforin knockout T cells (*Prf1*$^{-/-}$), which lack any killing activity, *k* is close to zero, and since we did not impose any restriction on it, *k* may become negative (see Fig. M1, below).

The per capita killing rate (PCKR) is defined here as the number of killed cells divided by the T cell number and the time of the experiment:

$$PCKR\ (T,t) = \frac{I(0) - I(t)}{T \times t}$$

where *I(t)* is the number of infected cells at the time point *t*. We did not observe any killing activity during the first 10 hours after injection of T cells. Ignoring this would potentially underestimate the PCKR and *k*. Therefore, we reduce the actual duration of T cell activity correspondingly:

$$PCKR\left(T, \frac{14}{24}[day]\right) = \frac{I(0) - I\left(\frac{14}{24}\ [day]\right)}{T \times \frac{14}{24}\ [day]}$$

The PCKR, in contrast to the parameter *k*, depends on the number of T cells (see Fig. M2, below) and the time of the experiment. Note that *k* is more suitable for comparison of the killing activity of T cells in different experiments. However, for the purpose of illustration, in this study we show PCKRs computed for one T cell and I_0 infected cells obtained from fitting the data from Figure 6A-C. For every experimental condition we calculated the PCKRs based on the estimated values of *k* and estimated its confidence interval using the 95% confidence interval of *k*.

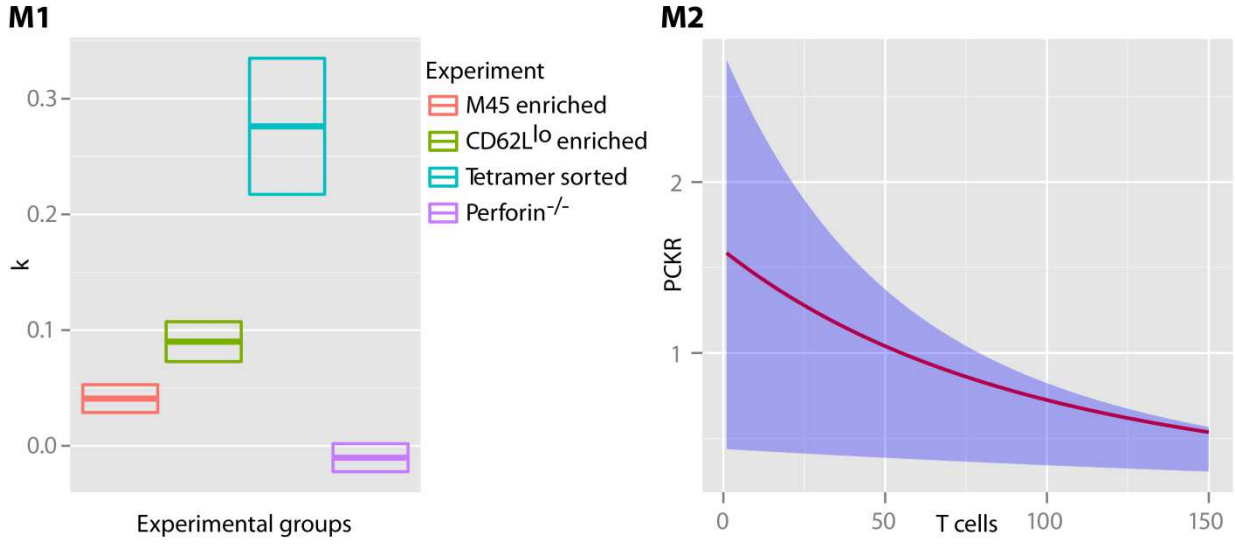

Figure **M1:** Estimations of the parameter k ($[day]^{-1}[cell]^{-1}$) and its 95% confidence interval corresponding to four experimental conditions. Figure **M2**: An example of dependence of PCKR on the number of T cell (M45-enriched). Shaded area corresponds to 95% confidence interval.

Supplemental References

Altman, J. D., Moss, P. A., Goulder, P. J., Barouch, D. H., McHeyzer-Williams, M. G., Bell, J. I., McMichael, A. J., and Davis, M. M. (1996). Phenotypic analysis of antigen-specific T lymphocytes. Science *274*, 94-96.

Aramburu, J., Garcia-Cozar, F., Raghavan, A., Okamura, H., Rao, A., and Hogan, P. G. (1998). Selective inhibition of NFAT activation by a peptide spanning the calcineurin targeting site of NFAT. Mol Cell *1*, 627-637.

Braun, A., Worbs, T., Moschovakis, G. L., Halle, S., Hoffmann, K., Bolter, J., Munk, A., and Forster, R. (2011). Afferent lymph-derived T cells and DCs use different chemokine receptor CCR7-dependent routes for entry into the lymph node and intranodal migration. Nat Immunol *12*, 879-887.

Chen, T. W., Wardill, T. J., Sun, Y., Pulver, S. R., Renninger, S. L., Baohan, A., Schreiter, E. R., Kerr, R. A., Orger, M. B., Jayaraman, V., *et al.* (2013). Ultrasensitive fluorescent proteins for imaging neuronal activity. Nature *499*, 295-300.

G.J. Nehls, G. G. A. (1973). Procedures for handling aerometric data. Journal of the Air Pollution Control Association *23*, 180–184.

Galla, M., Schambach, A., and Baum, C. (2013). Retrovirus-based mRNA transfer for transient cell manipulation. Methods Mol Biol *969*, 139-161.

Halle, S., Dujardin, H. C., Bakocevic, N., Fleige, H., Danzer, H., Willenzon, S., Suezer, Y., Hämmerling, G., Garbi, N., Sutter, G., *et al.* (2009). Induced bronchus-associated lymphoid tissue serves as a general priming site for T cells and is maintained by dendritic cells. J Exp Med *206*, 2593-2601.

Kremer, M., Volz, A., Kreijtz, J. H., Fux, R., Lehmann, M. H., and Sutter, G. (2012). Easy and efficient protocols for working with recombinant vaccinia virus MVA. Methods Mol Biol *890*, 59-92.

Lehmann, M. H., Kastenmuller, W., Kandemir, J. D., Brandt, F., Suezer, Y., and Sutter, G. (2009). Modified vaccinia virus ankara triggers chemotaxis of monocytes and early respiratory immigration of leukocytes by induction of CCL2 expression. J Virol *83*, 2540-2552.

Marquardt, A., Halle, S., Seckert, C. K., Lemmermann, N. A., Veres, T. Z., Braun, A., Maus, U. A., Forster, R., Reddehase, M. J., Messerle, M., and Busche, A. (2011). Single cell detection of latent cytomegalovirus reactivation in host tissue. J Gen Virol *92*, 1279-1291.

Morita, S., Kojima, T., and Kitamura, T. (2000). Plat-E: an efficient and stable system for transient packaging of retroviruses. Gene Ther *7*, 1063-1066.

Motulsky, H. J., and Brown, R. E. (2006). Detecting outliers when fitting data with nonlinear regression - a new method based on robust nonlinear regression and the false discovery rate. BMC Bioinformatics *7*, 123.

Munks, M. W., Gold, M. C., Zajac, A. L., Doom, C. M., Morello, C. S., Spector, D. H., and Hill, A. B. (2006). Genome-wide analysis reveals a highly diverse CD8 T cell response to murine cytomegalovirus. J immunol *176*, 3760-3766.

Nam, H. S., and Benezra, R. (2009). High levels of Id1 expression define B1 type adult neural stem cells. Cell Stem Cell *5*, 515-526.

R Core Team (2015). R: A Language and Environment for Statistical Computing.
Tischer, B. K., Smith, G. A., and Osterrieder, N. (2010). En passant mutagenesis: a two step markerless red recombination system. Methods Mol Biol *634*, 421-430.